

THE POWER SPECTRUM OF RICH CLUSTERS ON NEAR-GIGAPARSEC SCALES

CHRISTOPHER J. MILLER AND DAVID J. BATUSKI

Department of Physics & Astronomy, University of Maine

Draft version October 27, 2018

ABSTRACT

Recently, there have been numerous analyses of the redshift space power spectrum of rich clusters of galaxies. Some of these analyses indicate a “bump” in the Abell/ACO cluster power spectrum around $k = 0.05h\text{Mpc}^{-1}$. Such a feature in the power spectrum excludes most standard formation models and indicates possible periodicity in the distribution of large-scale structure. However, the data used in detecting this peak include clusters with estimated redshifts and/or clusters outside of Abell’s (1958) statistical sample, *i.e.* $R = 0$ clusters. Here, we present estimates of the redshift-space power spectrum for a newly expanded sample of 637 $R \geq 1$ Abell/ACO clusters which has a constant number density to $z = 0.10$ in the Southern Hemisphere and a nearly constant number density to $z = 0.14$ in the Northern Hemisphere. The volume sampled, $\sim 10^8 h^{-3} \text{Mpc}^3$, is large enough to accurately calculate the power per mode to scales approaching $10^3 h^{-1} \text{Mpc}$. We find the shape of the power spectrum is a power-law on scales $0.02 \leq k \leq 0.10 h\text{Mpc}^{-1}$, with enhanced power over less rare clusters such as APM clusters. The power-law here follows $n = -1.4$. The power spectrum is essentially featureless, although we do see a dip near $k = 0.04 h\text{Mpc}^{-1}$ which cannot be considered statistically significant based on this data alone. We do not detect a narrow peak at $k \sim 0.05 h\text{Mpc}^{-1}$ and there is no evidence for a turn-over in the power spectrum as has been previously reported. We compare the shape of the Abell/ACO rich cluster power spectrum to various linear models.

1. INTRODUCTION

There has recently been a renewed interest in accurately determining the power spectrum of matter distribution scales greater than $100h^{-1}\text{Mpc}$; in part due to the increased number of clusters with measured redshifts and the large volumes they trace. The power spectrum for the galaxy distribution has been determined many times for many different classes of galaxies. However, most galaxy surveys lack the volume necessary for the accurate quantification of power on large-scales (*e.g.* the Las Campanas Redshift Survey (Lin *et al.* 1996-hereafter LCRS) or the Stromlo-APM survey (Tadros & Efstathiou 1996). A summary of the results from these analyses is that the redshift-space power spectra roughly agree on scales $\lambda (= 2\pi/k) < 100h^{-1}\text{Mpc}$. In this region, $P(k) \propto k^n$ and $n \sim -2$. (Of course, the amplitude of the power spectra depends on the samples of galaxy examined which provides strong evidence for a luminosity bias (see *e.g.* Vogele *et al.* 1992 and Park *et al.* 1994)). However, on scales $\lambda > 100h^{-1}\text{Mpc}$, there is much less agreement. For example, some galaxy samples, such as from the LCRS and the Automated Plate Machine (APM) 2d and 3d surveys show a broad flattening around $k = 0.05h\text{Mpc}^{-1}$ although no distinct maximum can be found within convincing statistical bounds (LCRS; Tadros and Efstathiou 1996; Peacock 1997; Gatzanaga & Baugh 1998). However, Landy *et al.* (1996) find a distinct peak in $P(k)$ for a 2 dimensional analysis of the LCRS and Broadhurst *et al.* (1990) find a peak near $\lambda = 130h^{-1}\text{Mpc}$ in a deep pencil beam survey.

Some Abell/ACO cluster analyses also show a peak around $k \sim 0.05h\text{Mpc}^{-1}$ (Retzlaff *et al.* 1998; Einasto *et al.* 1997-hereafter E97). Yet other cluster analyses only show a smooth turnover in the power spectrum to its scale-invariant ($n = 1$) form. For instance, the APM clus-

ters, examined by Tadros, Efstathiou and Dalton (1998-hereafter TED98) show a maximum in $P(k)$ at the smaller value of $k \sim 0.03h\text{Mpc}^{-1}$ and no distinct “bump” at $k = 0.05h\text{Mpc}^{-1}$. Also, Peacock & West (1992) and Jing & Valdarnini (1993) find a break in the Abell cluster power spectrum near $k = 0.05h\text{Mpc}^{-1}$, but no distinct peak in power. An excellent review of the power spectra for different galaxy species can be found in Einasto *et al.* (1999-hereafter E99). E99 determine a mean power spectrum for all galaxies for a large range in wavenumber. They do this by using the APM 2d power spectra on small scales, and by averaging over numerous samples on large scales and then normalizing to the APM 2d power.

If a narrow peak in power near $k \sim 0.05h\text{Mpc}^{-1}$ is a real feature of the power spectrum in general, most current models of structure formation (in the quasi-linear regime) become invalid (E99). While baryonic signatures can produce features in the power spectrum, those features are oscillatory and they do not produce a singular, narrow peak as seen in some of the current data. Eisenstein *et al.* (1998) examined this prospect and found that no selection of cosmological parameters reproduces the power spectrum as seen in E97. However, Gramann & Suhhonenko (1999) suggest that an inflationary scenario with a scalar field having a localized step-like feature can reproduce the power spectrum of clusters. However, in this work, we show that the peak in the cluster power spectrum is not present in larger (in volume and in number) cluster samples after excluding less reliable data (such as $R = 0$ Abell/ACO clusters and clusters with estimated redshifts).

Our aim in this paper is to provide an estimate for the power spectrum of Abell/ACO clusters that is based on a complete and fair sample. Both Retzlaff *et al.* and

E97 use $R = 0$ clusters in their determination of $P(k)$. Einasto *et al.* (1994) have argued that $R = 0$ clusters do not contaminate studies of large-scale structure because the multiplicity of superclusters is independent of richness and the mean separation distances for $R = 0$ and $R \geq 1$ clusters are very similar. However, $R = 0$ clusters were not cataloged in a systematic way and were never meant to be examined in a statistical manner due to their incompleteness (Abell 1958). In addition, many researchers have found line-of-sight anisotropies in $R = 0$ cluster samples (Sutherland 1988; Efstathiou *et al.* 1992; Peacock & West 1992). Therefore, the use of $R = 0$ clusters in the determination of $P(k)$ is highly suspect. E97 have also used a large number (435 out of 1305 clusters) of estimated redshifts in their determination of $P(k)$. We also suspect that E97 used a large number of cluster redshifts with only one measured galaxy. Miller *et al.* (1999a) show that cluster velocities with one measured galaxy are in error by more than 2500 km s^{-1} 14% of the time. Of course, estimated redshifts are only accurate to at best 25%. Thus, the statistical certainty of any large-scale structure analyses based on the cluster samples with a large number of estimated or poorly determined redshifts must also be taken with caution.

2. THE CLUSTER SAMPLE

We examine Abell/ACO clusters across the entire sky excluding the galactic plane *i.e.* $|b| > 30^\circ$. We only consider $R \geq 1$ clusters (with measured redshifts) since they were defined by Abell (1958) as members of his statistically complete sample. Recently, Miller *et al.* (1999a,b) examined similar subsets of $R \geq 1$ clusters for projection effects, line-of-sight anisotropies, and spatial correlations. We summarize their results below.

The Abell/ACO $R \geq 1$ cluster dataset has significant advantages over other cluster samples (including those with $R = 0$ clusters as well as APM clusters). With the advent of multi-fiber spectroscopy, nearly all rich Abell/ACO clusters within $z = 0.10$ now have multiple galaxy determined redshifts (Slingsend *et al.* 1998; Katgert *et al.* 1996). Multiple redshifts have allowed for more accurate determinations of the extent of projection effects and Miller *et al.* 1999a report that at most, 10% of Abell/ACO clusters suffer from moderate to severe foreground/background contamination. The lack of projection effects for $R \geq 1$ clusters is also apparent from the 89% X-ray emission detection rate by Voges *et al.* 1999. Miller *et al.* (1999a,b) also show that there is very little line-of-sight anisotropy in the $R \geq 1$ Abell/ACO cluster samples - comparable to the APM cluster catalog (Dalton *et al.* 1994). This is in sharp contrast to $R \geq 0$ samples and even some modern X-ray selected/confirmed cluster samples (see e.g. Efstathiou *et al.* 1992, Peacock & West 1992, and Miller *et al.* 1999b).

Vogeley (1998) recently pointed out how Galactic extinction could add “false” power to structure analyses based on large galaxy samples (such as the Sloan Digital Sky Survey). While clusters should not be affected as strongly as individual galaxies, it is still worth examining extinction effects within our cluster sample. In 1996, Nichol and Connolly used the Stark *et al.* 1992 HI maps to report that some samples of Abell clusters significantly anti-correlate with regions of high galactic neutral hydro-

gen density. Recently, Schlegel, Finkbeiner, and Davis (1998) have created HI extinction maps of the entire sky with much greater resolution than the Stark HI maps. We use these new maps to re-examine and confirm the Nichol and Connolly results. We also examine a volume-limited ($z = 0.10$) sample of Abell/ACO clusters. Using a Kolmogorov-Smirnov (K-S) test, we compare the E(B-V) extinctions for positions centered on the Abell/ACO clusters to E(B-V) extinctions for several thousand randomly selection positions. We find that the probability that our clusters were drawn from a random selection of E(B-V) extinctions is 10%. In other words, the average extinction within our Abell/ACO clusters is smaller than for the random positions, but not significantly so. For comparison, Nichol and Connolly found only a 2% probability that the Postman, Huchra, and Geller (1992) Abell/ACO clusters (with $|b| \geq 30^\circ$ and $R \geq 1$) were drawn from a random sampling of E(B-V) extinctions. The effect that galactic extinction would have on a power spectrum should not be as strong for clusters as it would be for galaxies. Cluster galaxies have a wide range of magnitudes, and while some dimmer galaxies within a cluster may be missed due to extinction, the majority of bright galaxies will still be counted. When we created our volume-limited samples, we are including those clusters that appear dim as a result of galactic extinction (as opposed to a magnitude-limited survey which would exclude those clusters). The lack of statistically significant evidence that our clusters are corrupted by extinction, and the use of a volume-limited sample (with $|b| \geq 30^\circ$), convinces us that we can ignore any extinction effects in our analyses. However, to be certain that extinction is not altering the shape or amplitude of our redshift-space power spectrum, we will model the extinction distribution of our clusters in our random catalogs for one of our two PS estimation methods (see method (b) below).

An additional argument for the completeness of $R \geq 1$ Abell/ACO clusters is provided by their spatial number density as shown in Figure 1. We use clusters of all magnitudes and use the same methods as Miller *et al.* (1999a) to calculate and bin the cluster number densities. Notice in Figure 1 that the sample has a nearly constant density out to $z = 0.10$ and that the density only drops by a factor of 0.58 out to $z = 0.14$. [Note: The bump in the density at $z \sim 0.07$ is mostly due to the Corona Borealis Supercluster.] In Figure 1, we fit three different functions to the number density: a three-parameter number function (as in FKP), a power-law for $z \geq 0.10$, and a step-function. The best-fit produces $\chi^2_{red} = 2$ for the number function.

Using cluster redshifts from the literature as well as ~ 100 as yet unpublished redshifts from the MX Survey Extension (Miller *et al.* 2000), we have created a sample of 637 $R \geq 1$ Abell/ACO clusters with $|b| \geq 30^\circ$. The MX Survey provides a much deeper (in both magnitude and in redshift) catalog of Northern Hemisphere cluster redshifts than is currently available for the Southern Hemisphere ACO clusters (see e.g. Miller *et al.* 1999; Katgert *et al.* 1996). Therefore, we exclude any cluster beyond $z = 0.10$ in the south ($\delta \leq -27^\circ$) and beyond $z = 0.14$ in the north ($\delta \geq -27^\circ$). Several researchers have noted discrepancies between the richness counts of the Abell and ACO catalogs (see Miller *et al.* (1999) for a discussion). Therefore, we also measure $P(k)$ for a subset of our data that excludes

all ACO clusters with $N_{gal} < 55$ (where N_{gal} is the number of galaxies used to determine the richness as given in ACO and $N_{gal} \geq 50$ corresponds to $R \geq 1$). This richness cut excludes 30 ACO clusters from our sample.

This is the largest cluster sample compiled to date for large-scale structure analyses. The survey volume covers $1.2 \times 10^8 h^{-3} \text{Mpc}^3$ and is nearly four times larger than the APM cluster survey (Dalton *et al.* 1994) and the Retzlaff *et al.* (1998) Abell/ACO survey. Additionally, only $\sim 10\%$ of our cluster redshifts are based on one measured galaxy redshift. We calculate distances to the clusters using a Friedmann Universe with $q_0 = 0$ and $H_0 = 100 \text{ km s}^{-1} \text{ Mpc}^{-1}$. The choice of q_0 makes little difference in our results (see also Retzlaff *et al.* 1998).

When a cluster dataset goes as deep as the one used here, and has been created in a somewhat piecemeal fashion, we must be very confident that the cluster observations used in this sample are more or less isotropic in volume, and that we are not including large sections of the sky that go deeper (in magnitude) than others. We address this concern figuratively in Figure 2, by examining the fraction of observed to total cataloged clusters. In this sky plot (in galactic coordinates), we show Abell clusters with $z = 0.10$ (filled circles), Abell clusters within $0.10 < z \leq 0.14$ (open circles), and ACO clusters within $z = 0.10$ (stars). We can divide the sky into quadrants with two sections in the north and two in the south (each separated at $l = 180^\circ$) and examine nearby ($z \leq 0.10$) and distant ($0.10 < z \leq 0.14$) clusters separately. From Figure 2, we see reasonably fair coverage throughout the entire sky in both redshift ranges (recall that the southern right quadrant only goes to $z = 0.10$). Quantitatively, we present in Table 1 the number of clusters available in each quadrant cataloged by Abell/ACO, and the number of clusters observed in each quadrant. Note that the fractional coverages in each of the sections are very similar. The mean fractional coverage (including both near and far quadrants) is 0.138 ± 0.019 , so that the number of clusters within the more distant, northern right quadrant is only 1.5σ smaller than the mean. Table 1 provides clear evidence that the sky coverage for our cluster sample is not observationally biased towards certain regions.

After accounting for projection effects, line-of-sight anisotropies, X-ray identifications, HI column density variations, a constant number density, and fair sky coverage, this is the largest, most complete, and fairly sampled distribution of matter in the local Universe. We assume that clusters are biased tracers of mass (Kaiser 1986; Peacock & Dodds 1994) and that in the end, we may compare the shape of our power spectrum to those of typical cosmological models.

3. METHODS AND ANALYSES

We utilize two different methods to estimate $P(k)$ in redshift-space. Both methods follow the same basic idea: directly sum the plane wave contributions from each cluster, account for appropriate weights and the shape of the volume, compute the square of the modulus of each mode and subtract off the shot noise. The resultant power spectrum is the estimated variance of the density contrast $|\delta(k)|^2$. The power spectrum is accurate only to some limiting scale, specified by k_{min} , which is constrained by the size and shape of the volume examined. The differ-

ences between the two methods arise when accounting for the weighting scheme and the shape of the volume. We also point out that Tegmark *et al.* (1998) have recently presented an alternative method for measuring $P(k)$ for large datasets (such as the Sloan Digital Sky Survey). As discussed in detail in Tegmark *et al.*, they advocate the use of standard Fourier techniques on small scales, a pixelized quadratic matrix method on large-scales, and also a Karhunen - Loeve (KL) eigenmode analysis to probe redshift-space anisotropies. While the Tegmark *et al.* power spectrum estimation method is undoubtedly more refined than the methods used here, we are more interested in comparing results from the most commonly used techniques (and also allowing our results to be compared to previous cluster $P(k)$ measurements). Also, the methods described in Tegmark *et al.* are designed for large datasets (e.g. several 100,000 points) and we would not expect a large advantage in our smaller samples.

The first method we use was originally applied by Voegeley *et al.* (1992), Park *et al.* (1994) and da Costa *et al.* (1994) to the CfA2 redshift survey (Geller & Huchra 1989). This method is also described in LCRS and Fisher *et al.* 1993. Most recently, this method was used and described by Retzlaff *et al.* (1998) on a sample of Abell/ACO clusters. Briefly, the estimated power spectrum convolved with the window function can be written as follows:

$$\hat{P}_a(k) = \frac{V}{1 - |\hat{W}(k)|^2} [\hat{\Pi}(k) - \hat{S}]. \quad (1)$$

The first factor in Equation 1 accounts for the systematic under-estimation of $P(k)$ at small values of k due to normalization biases and the shape of the window, also known as large-scale power damping (Peacock & Nicholson 1991). The first term in brackets, $\hat{\Pi}$ is the squared-modulus of the Fourier transform of the density contrast, $\delta(\mathbf{r})$, minus the Window Function, or the estimated power. $\hat{\Pi}$ is a discrete quantity that includes shot noise \hat{S} which we must subtract off. The estimate of the power, $\hat{P}_a(k)$, is convolved with the Window function, $\hat{W}(k)$.

In practice, we calculate $\hat{W}(k)$ separately for as many points as is feasible (in this case 3×10^5 random points) and average over 1000 directions of k . The window function is presented in Figure 3. We calculate $|\hat{W}(k)|^2$ using points randomly distributed in our volume and also with the same redshift and extinction distribution as our real data (the redshift distribution is smoothed with a Gaussian to remove any large-scale structure). Figure 3 shows that the shape of $|\hat{W}(k)|^2$ changes very little as we adjust the random distribution within our volume. We also calculate $|\hat{W}(k)|^2$ for a volume that encompasses only one hemisphere out to $z = 0.14$. We see that, as the volume becomes more asymmetric, significant differences between the window functions appear. The ‘‘bumps’’ seen in $|\hat{W}(k)|^2$ are a direct result of a volume-limited, spherically symmetric survey, and have little effect on the PS estimation, so long as their relative heights are much smaller than the largest $|\hat{W}(k)|^2$ used. These ‘‘bumps’’ are an indicator that the survey window is spherically symmetric and that averaging over all directions of \mathbf{k} is appropriate. This is not typically the case in previous (non-Abell/ACO)

$P(k)$ analyses (see Tegark (1995) for a good discussion of window functions).

The smallest k that can be accurately probed depends on the value of $|\hat{W}(k)|^2$ and how it convolves with the real power spectrum (see Lin et al. 1996). Recall,

$$\langle P_{estimated}(k) \rangle \propto \int |\hat{W}(\mathbf{k} - \mathbf{k}')|^2 P_{true}(\mathbf{k}') k'^2 dk'. \quad (2)$$

Ideally, for all values of k probed, the integrand of Equation (2) will be sharply peaked at $k = k'$. In Figure 4, we plot the integrand of Equation (2) assuming a constant $P(k)$. We find that the shape of our volume does not affect our analyses for $k > \sim 0.015h\text{Mpc}^{-1}$. For k smaller than this limit, we see that “leakage” occurs and power from larger k slips into our measurements. Figure 4 also shows that if uncorrelated modes of $P(k)$ are required, we should separate our bins by $\delta k = 0.015$. Our choice of $k_{min} = 0.015h\text{Mpc}^{-1}$ is a conservative limit, since most past analyses of $P(k)$ have stopped where $|\hat{W}(k)|^2 = 0.1$ (e.g. Peacock and Nicholson 1991; Vogeley et al. 1992; Retzlaff et al. 1998). The value of $|\hat{W}(k)|^2$ for our analysis at k_{min} is only $0.05h\text{Mpc}^{-1}$.

The weights for each cluster originate in the estimation of the density contrast,

$$\hat{\delta}(r) = \frac{1}{N} \sum_i \frac{\delta^3(\mathbf{r} - \mathbf{r}_i)}{\phi(r_i)} - 1 \quad (3)$$

where $\phi(\mathbf{r}) = \psi(b)\varphi(z)$ is the selection function which accounts for galactic obscuration and redshift selection. We use $\psi(b) = 10^{\gamma(1 - csc|b|)}$ with $\gamma = 0.32$ for the latitude selection function (see Postman, Huchra, and Geller 1992). The selection function in z is determined separately for the three different number density models used in Figure 1. We find that the choice of number-density fit has little on the PS estimation.

The second method we use was derived by Feldman, Kaiser, & Peacock (1994-hereafter FKP). TED96 use a very similar approach in their analysis of APM clusters. Here, the power spectrum is:

$$\hat{P}_b(k) = |F(\mathbf{k})|^2 - P_{shot} \quad (4)$$

where $F(k)$ is the Fourier transform of the normalized and weighted galaxy fluctuation field:

$$F(\mathbf{r}) = \frac{\mathbf{w}(\mathbf{r})[\mathbf{n}_c(\mathbf{r}) - \alpha \mathbf{n}_s(\mathbf{r})]}{[\int \mathbf{d}^3\mathbf{r} \bar{n}^2(\mathbf{r}) \mathbf{w}^2(\mathbf{r})]^{1/2}} \quad (5)$$

In these equations, n_c and n_s represent the number densities of the cluster sample and a randomly generated synthetic catalog respectively. The number of points we use in the random catalog is 500 times that of the real data so $\alpha = \frac{1}{500}$ (we note that there is no difference in the power spectrum results for random catalogs with 100 times as many points). P_{shot} is again, the power due to shot noise from a discrete sample and is determined as in FKP. In this method, we model the redshift selection of our random catalogs from the redshifts of the real data, smoothed with a Gaussian of width 3000 km s^{-1} . The weights for the individual clusters (real and synthetic) are determined from

$$w_o(r) = \frac{1}{1 + n(r)P_{init}(k)}. \quad (6)$$

To create the extinction adjusted random catalogs, we draw from regions in the sky that have the same extinction distribution as our real data using the Schlegel et al. (1998) maps. We find little difference in our $P(k)$ when we apply no extinction correction. To determine $n(r)$ used in the weighting factor, we use the three different number density fits (as given in Figure 1). Again, we find that the choice of number density fit has little effect on the PS estimation.

The weighting scheme for $P_b(k)$ depends on *a priori* knowledge of $P(k)$ at all scales. We choose different values of $P_{init}(k)$ ($5, 10, 30, 60 \times 10^4 h^{-3} \text{Mpc}^3$) for the cluster weights and find that there is little difference in the amplitude (~ 1.5 times) of $P_b(k)$ between $P_{init} = 5$ and $60 \times 10^4 h^{-3} \text{Mpc}^3$ and so we adopt $P_{init} = 30 \times 10^4 h^{-3} \text{Mpc}^3$ in all further $P_b(k)$ results. We calculate errors on $P_b(k)$ using those methods of FKP (equation 2.4.6).

In Figure 5, we compare all of our calculations of $P(k)$. In the top panel of Figure 5, we plot $P_a(k)$ using the three different number density functions. We also measure $P(k)$ for the richness adjusted sample. We plot the same for $P_b(k)$ in the middle panel of Figure 5. In all cases, we find very little difference in our $P(k)$ estimations. In the bottom panel of Figure 5 we compare $P_a(k)$ to $P_b(k)$ using the number function as our density fit. Here, we do see some small differences in the measured power at k less than $0.02h\text{Mpc}^{-1}$, however both spectra estimates are within the 1σ error. The lack of difference between $P_a(k)$ and $P_b(k)$ is a direct result of the stability of the methods and the well defined number density and symmetric volume of the cluster sample.

4. DISCUSSION

There are two striking results regarding the power spectrum of rich Abell/ACO clusters. (1) While we do see a dip in power near $k = 0.4h \text{ Mpc}^{-1}$, it is not statistically significant. The measured power spectrum is essentially featureless and there is no narrow peak in the power spectrum as has been reported in E97 and Retzlaff *et al.* (1998). (2) The other difference is that there is increasing power to very large scales ($k = 0.015h\text{Mpc}^{-1}$ or $\sim 400h^{-1}\text{Mpc}$). In past analyses of the power spectrum, most authors have reported the (weak) detection of a turnover in the power spectrum (see section 1). However, the turnover has always occurred very near the largest scales accessible in their volumes. [Note: other preliminary analyses of the PS on scales $k < 0.05h\text{Mpc}^{-1}$ are also showing this increase in power (Guzzo et al. 1999; Hamilton and Tegmark 2000; Efstathiou and Moody 2000)]. The power spectrum is roughly a power-law on scales $0.02 \leq k < 0.10h\text{Mpc}^{-1}$ with $P(k) \propto k^{-1.4}$.

In Figure 6, we compare our results to two other cluster sample power spectrum analyses, the APM cluster sample of TED98, and the $R \geq 0$ Abell/ACO sample of Retzlaff et al. (1998). Figure 6 shows that the shapes of $P(k)$ for these three different cluster samples are remarkably similar in the range $0.04 \leq k \leq 0.15h\text{Mpc}^{-1}$. The higher amplitude for our sample of $R \geq 1$ clusters is expected according to hierarchical clustering schemes (Kaiser 1986) and larger bias found in richer clusters (see Peacock

and Dodds 1994). We have recalculated the Retzlaff *et al.* (1998) Abell/ACO cluster sample using the methods for $P_a(k)$. We do this in part as a check on our methods and also to independently confirm their results of a peak near $k = 0.05h\text{Mpc}^{-1}$ and a turnover thereafter. The Retzlaff *et al.* sample includes all Abell/ACO clusters within $240h^{-1}\text{Mpc}$ and outside $|b| \geq 30^\circ$. We find 412 clusters which meet this criteria (compared to their 417 clusters—the difference we attribute to minor variations in a few cluster redshifts near the survey boundaries). Our results, not surprisingly, are identical to those published in Retzlaff *et al.* (1998) since our method for determining $P_a(k)$ is identical to theirs. For this determination of $P_a(k)$ (*i.e.* using $R = 0$ clusters and a much smaller volume), we also see a peak in the power spectrum at $k = 0.05h\text{Mpc}^{-1}$ and a turnover thereafter. As pointed out by Retzlaff *et al.*, this peak is not statistically significant. As a further examination of this issue, we plot in Figure 6 $P_b(k)$ for a smaller cluster sample, volume-limited in the north and south to $z = 0.10$. For this sample, we can only detect power to $k_{min} \sim 0.035h\text{Mpc}^{-1}$. For k greater than $0.035h\text{Mpc}^{-1}$ we find little difference between this sample and the larger one. But we can no longer probe on the scales where we expect $P(k)$ to continue its rise. Thus, one could conclude that a turn-over has been found, when in fact a larger (in size and number) sample shows that the power continues to rise for $k < 0.03h\text{Mpc}^{-1}$.

4.1. Comparisons to Linear Theory

We also compare our power spectrum results to those of linear theory created by CMBFAST (Seljak & Zaldarriaga 1996). We consider three Cold Dark Matter (CDM) variants, flat, open and with a vacuum density (ΛCDM), and a Mixed Dark Matter (MDM) model. For the CDM cases, we choose $\Omega_b = 0.02$, in accordance with Schramm & Turner (1998). For the open case, we choose $\Omega_0 = \Omega_b + \Omega_{CDM} = 0.2$ in accordance with Bahcall (1997). For the ΛCDM model, we choose $\Omega_{CDM} = 0.18$ and $\Omega_{vacuum} = 0.80$ so that $\Omega_b + \Omega_{CDM} + \Omega_{vacuum} = 1$. For the MDM model, we choose $H_0 = 50\text{km s}^{-1}\text{Mpc}^{-1}$ with $\Omega_b = 0.05$, $\Omega_{CDM} = 0.35$ and $\Omega_\nu = 0.3$ (where Ω_ν is the massive neutrino density). The CMBFAST package normalizes the amplitude of generated spectra to the Bunn and White (1997) four-year COBE normalization. However, in this work, we are only concerned with the *shape* of the power spectrum. We are motivated by our assumption that clusters are biased tracers of the mass distribution and therefore the shape of the cluster power spectrum should be similar to that of the matter power spectrum. In Figure 7, we present the amplitude shifted linear models in comparison to our empirically determined power spectra. As a result of the known similarities in the shapes of the ΛCDM models and low matter density open CDM models, we find that both fit the shape of the rich Abell/ACO cluster power spectrum to $k_{min} = 0.015h\text{Mpc}^{-1}$ or $400h^{-1}\text{Mpc}$ extremely well (see Table 2). On the largest scales, the MDM model lacks power over a wide range of k ($0.015 \leq k \leq 0.03h\text{Mpc}^{-1}$) to match our cluster data. TED98 found that ΛCDM linear models did not have enough power on large scales to match the APM cluster power spectrum. Instead, they find a much better fit for a mixed dark matter (MDM) model. We point out that the ΛCDM model in Figure 7 of

TED98 does provide an excellent fit to the APM cluster data if their last data point at $k = 0.02h\text{Mpc}^{-1}$ (where the error is rather large) is excluded.

5. CONCLUSION

The agreement between the shapes of $P(k)$ for the four different samples shown in Figure 6 (from $k = 0.05$ to $0.15h\text{Mpc}^{-1}$), provides further evidence that clusters are tracers of the peaks of the underlying luminous mass distribution. While there is a great deal of volume-overlap in these four samples, they are made up of significantly different luminous objects (from very poor APM clusters to the richest Abell clusters). For instance, the Retzlaff *et al.* (1998) Abell/ACO sample contains at most 253 $R \geq 1$ clusters, while the remaining 218 are $R \geq 0$. Our sample contains 637 $R \geq 1$ clusters. The APM sample of 364 clusters, contains even fewer $R \geq 1$ Abell clusters (~ 40). If all groups and clusters trace the underlying mass distribution in a similar way, then we would expect their respective power spectra to be similar in shape, and only the amplitude to vary.

Previous analyses of the cluster power spectrum have been plagued by three major problems: (1) uncertainties in the number density, (2) small volumes, and (3) irregularly shaped volumes. The sample analyzed in this work greatly improves upon each of these difficulties. Our Abell/ACO sample has a nearly constant number density throughout the entire volume. This is in stark contrast to most other sparse tracer surveys (such as the QDOT *IRAS* survey power spectrum of FKP and the Retzlaff *et al.* Abell/ACO cluster sample). Along with the number density, the large size of the volume and the semi-regular shape of the double-cone geometry, all contribute significantly to a more accurate determination of $P(k)$ on the largest scales. The reality of the power on scales $200 - 300h^{-1}\text{Mpc}$ is also becoming evident observationally. Batuski *et al.* 1999 have recently discovered two filamentary superclusters in the constellation of Aquarius that are as long as $75h^{-1}\text{Mpc}$ and $150h^{-1}\text{Mpc}$. As we peer out further into the local Universe, we continue to find structures on very large scales.

We have presented the redshift-space power spectrum for the largest galaxy cluster sample compiled to date. This sample has been examined extensively for projection effects, anisotropies, and observational selection effects and found to be a fair and complete sampling of biased matter in the local Universe. The volume and shape of the survey provide accurate and robust measurements of $P(k)$ over the wavenumber range $0.015 \leq k \leq 0.15h\text{Mpc}^{-1}$. From $k = 0.15$ down to $k = 0.05h\text{Mpc}^{-1}$, we find a similar shape to the power spectrum compared to other cluster samples such as the APM cluster survey and a smaller sample of $R \geq 0$ Abell/ACO clusters studied by Retzlaff *et al.* (1998). At smaller k , we do not find any statistically significant features in $P(k)$. Unlike previous cluster $P(k)$ analyses, we do not find any strong evidence for a turnover. We find that ΛCDM and low Ω_0 CDM linear models provide excellent fits to the rich cluster power spectrum.

Acknowledgments The authors wish to thank Adrian Melott and Daniel Eisenstein for helpful conversations. We also would like to acknowledge the role of the referee, Michael S. Vogeley, for his suggestions on improving the original manuscript. We also thank H. Tadros for supply-

ing the APM cluster PS in electronic form. CM was funded in part by NASA-EPSCoR through the Maine Science and

Technology Foundation.

REFERENCES

- Abell, G. O. 1958, *ApJS*, 3, 211
 Abell, G. O., Corwin, H. G., Olowin, R. P. 1989, *ApJS*, 70, 1 (ACO)
 Bahcall, N. 1997, in *Critical Dialogues in Cosmology*, ed. N. Turok, World Scientific, Singapore, 221
 Batuski, D.J., Miller, C.J., Slinglend, K.A., Balkowski, C., Maurogordato, S., Cayatte, V., Felenbok, P., and Olowin, R. 1999, *ApJ*, 520, 491
 Broadhurst, T.J., Ellis, R.S., Koo, D.C., & Szalay, A.S. 1990, *Nature*, 343, 726
 Bunn, E.F. & White, M. 1997, *ApJ*, 480, 6
 da Costa, L.N., Vogeley, M.S., Geller, M.J., Huchra, J.P., & Park, C. 1994, *ApJ*, 437, L1
 Dalton, G.B., Croft, R.A.C., Efstathiou, G., Sutherland, W.J., Maddox, S.J., and Davis, M. 1994, *MNRAS*, 271, 47
 Efstathiou, G., Dalton, G.B., Maddox, S.J., & Sutherland, W. 1992, *MNRAS*, 257, 125
 Efstathiou, G. and Moody, S.J. 2000, preprint astro-ph/0010478
 Einasto, J., Einasto, M., Gottlöber, S., Müller, V., Saar, V., Starobinsky, A.A., Tago, E., Tucker, D., Andernach, H., & Frisch, P. 1997, *Nature*, 385, 139 (E97)
 Einasto, J., Einasto, M., Tago, E., Starobinsky, A.A., Atri-Barandela, F., Müller, V., Knebe, A., & Cen, R. 1999, *ApJ*, 519, 469 (E99) Frisch, P. 1997, *Nature*, 385, 139 (E97)
 Einasto, M., Einasto, J., Tago, E., Dalton, G.B., & Andernach, H. 1994, *MNRAS*, 269, 301
 Eisenstein, D.J., Hu, W., Silk, J., and Szalay, A.S. 1998, *ApJ*, 494, L1
 Feldman, H.A., Kaiser, N. & Peacock, J.A. 1994, *ApJ*, 426, 23 (FKP)
 Fisher, K.B., Davis, M., Strauss, M.A., Yahil, A., & Huchra, J.P. 1993, *ApJ*, 402, 42
 Gatzagaña, E. & Baugh, C.M. 1998, *MNRAS*, 294, 229
 Geller, M. J. & Huchra, J. P. 1989, *Science*, 246, 897
 Gramann, M. & Suhhonenko, I. 1999, *ApJ*, 519, 433
 Hamilton, A.J.S. and Tegmark, M. 2000, submitted to *MNRAS*, astro-ph/0008392
 Guzzo, L. 1999, presented at *The Second Coral Sea Cosmology Conference*
 Hoyle, F., Baugh, C. M., Shanks, T., Ratcliffe, A. 1999, *MNRAS*, 309, 659
 Jing, Y.P. and Valdarnini, R. 1993, *ApJ*, 406, 6
 Kaiser, N. 1986, *MNRAS*, 222, 323
 Katgert, P., Mazure, A., Perea, J., den Hartog, R., Moles, M., Le Fevre, O., Dubath, P., Focardi, P., Rhee, G., Jones, B., Escalera, E., Biviano, A., Gerbal, D., Giuricin, G. 1996, *A & A*, 310, 8
 Landy, S.D., Shectman, S.A., Lin, H., Kirshner, R.P., Oemler, A.A., & Tucker, D. 1996, *ApJ*, 456, L1
 Lin, H., Kirshner, R.P., Shectman, S.A., Landy, S.D., Oemler, A., Tucker, D.L., & Schechter, P.L. 1996, *ApJ* 471, 617 (LCRS)
 Miller, C.J., Batuski, D.J., Slinglend, K.A., & Hill, J.M. 1999a, *ApJ*, 523, 492
 Miller, C.J., Ledlow, M.J. & Batuski, D.J. 1999b, *MNRAS*, submitted
 Miller, C.J., Krughoff, K.S., Slinglend, K.A., Batuski, D.J., & Hill, J.M. 1999c (in preparation)
 Nichol, R.C. & Connolly, A.J. 1996, *MNRAS*, 279, 521
 Park, C., Vogeley, M.S., Geller, M.J., & Huchra, J.P. 1994, *ApJ*, 431, 561
 Peacock, J.A. 1997, *MNRAS*, 285, 885
 Peacock, J.A. & Dodds, S.J. 1994, *MNRAS*, 267, 1020
 Peacock, J.A. & Nicholson, D. 1991, *MNRAS*, 253, 307
 Peacock, J.A. & West, M.J. 1992, *MNRAS*, 259, 494
 Postman, M., Huchra, J. P., & Geller, M. J. 1992, *ApJ*, 384, 404
 Retzlaff, J., Borgani, S., Gottlöber, S., Klypin, A., & Müller, V. 1998, *NewA*, 3, 631
 Schlegel, D.J., Finkbeiner, D.P., & Davis, M. 1998, *ApJ*, 500, 525
 Schramm, D.N. & Turner, M.S. 1998, *Rev. Mod. Phys.*, 70, 303
 Seljak, U. & Zaldarriaga, M. 1996, *ApJ*, 469, 437
 Slinglend, K.A., Batuski, D.J., Miller, C.M., Haase, S., Michaud, K., & Hill, J.M. 1998, *ApJS*, 115, 1
 Stark, A.A., Gammie, C.F., Wilson, R.W., Bally, J.L., Linke, R.A., Heiles, C., & Hurwitz, M. 1992, *ApJS*, 79, 77
 Sutherland, W. 1988, *MNRAS*, 234, 159
 Tadros, H., & Efstathiou, G. 1996, *MNRAS*, 282, 1381 (TE96)
 Tadros, H., Efstathiou, G., & Dalton, G. 1998, *MNRAS*, 296, 995 (TED98)
 Tegmark, M. 1995, *ApJ*, 455, 429
 Vogeley, M.S. 1998, in *The Evolving Universe*, Kluwer Academic Publishers, p. 395
 Vogeley, M.S., Park, C., Geller, M.J., & Huchra, J.P. 1992, *ApJ*, 391, L5
 Voges, W., Ledlow, M.J., Owen, F.N., & Burns J.O. 1999, *AJ*, submitted

TABLE 1
Sky Coverage

ℓ range	b range	z range	Number (all z) cataloged	Number with observed redshifts	Fraction ^a
$0^\circ \leq \ell < 180^\circ$	$30^\circ \leq b \leq 90^\circ$	$z \leq 0.10$	636	80	0.1257
$0^\circ \leq \ell < 180^\circ$	$30^\circ \leq b \leq 90^\circ$	$0.10 < z \leq 0.14$	636	86	0.1352
$180^\circ \leq \ell < 360^\circ$	$30^\circ \leq b \leq 90^\circ$	$z \leq 0.10$	503	78	0.1550
$180^\circ \leq \ell < 360^\circ$	$30^\circ \leq b \leq 90^\circ$	$0.10 < z \leq 0.14$	503	52	0.1034
$0^\circ \leq \ell < 180^\circ$	$-90^\circ \leq b \leq -30^\circ$	$z \leq 0.10$	608	95	0.1563
$0^\circ \leq \ell < 180^\circ$	$-90^\circ \leq b \leq -30^\circ$	$0.10 < z \leq 0.14$	608	84	0.1382
$180^\circ \leq \ell < 360^\circ$	$-90^\circ \leq b \leq -30^\circ$	$z \leq 0.10$	492	75	0.1524

^aFraction is the Number observed/ Number cataloged.

TABLE 2
Goodness-of-Fit to Linear Models

Model	$\chi^2_{reduced}$	DOF
Λ CDM ($H_o = 100\text{km s}^{-1}$)	0.65	8
Open CDM ($H_o = 100\text{km s}^{-1}$)	0.66	8
CDM ($H_o = 100\text{km s}^{-1}$)	4.55	8
MDM ($H_o = 50\text{km s}^{-1}$)	2.19	8

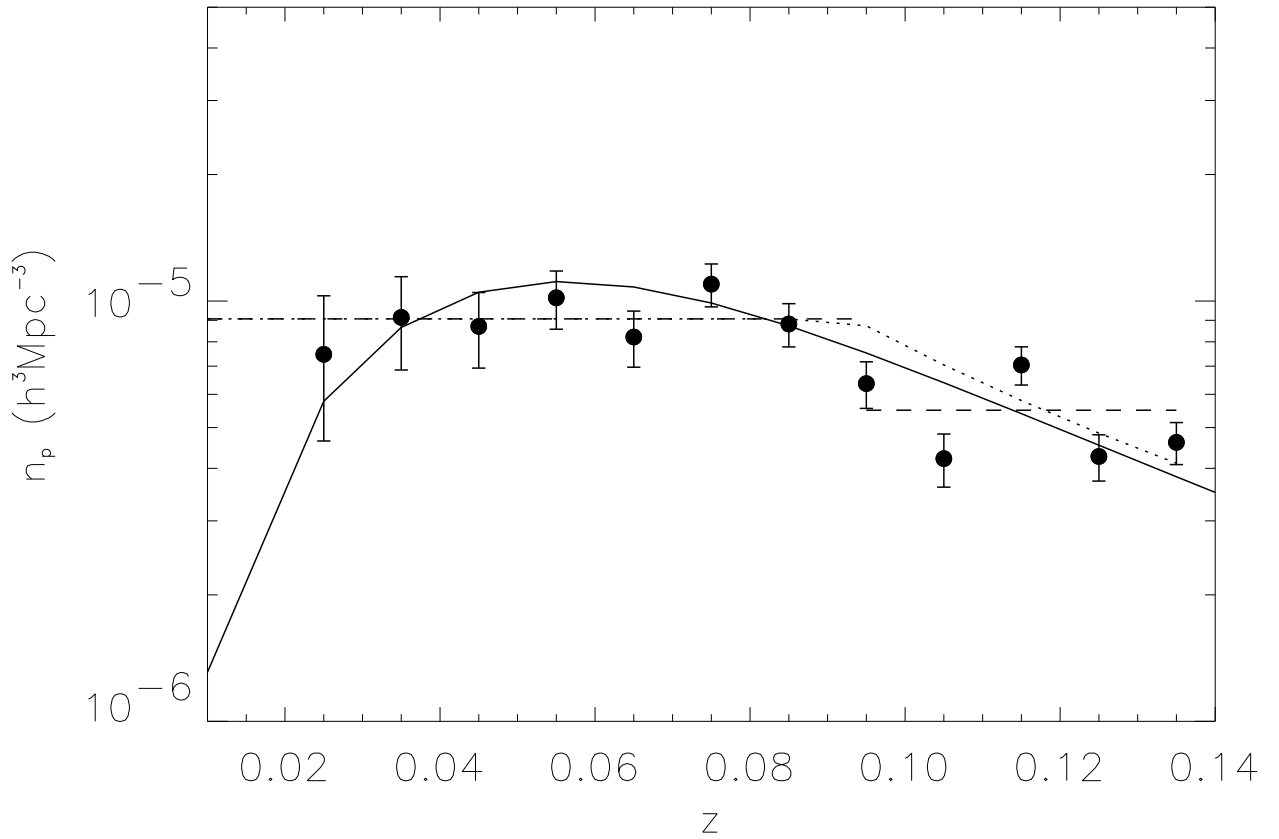


FIG. 1.— The proper number density as a function of redshift is presented for the Abell/ACO cluster sample. The lines are various fits to the data. The solid-line (having the lowest χ^2) is a three parameter number function. The dotted-line is for a power-law beyond $z = 0.01$. The dashed-line is for a step function. We find no significant differences in our PS analysis as a function of the number density function utilized.

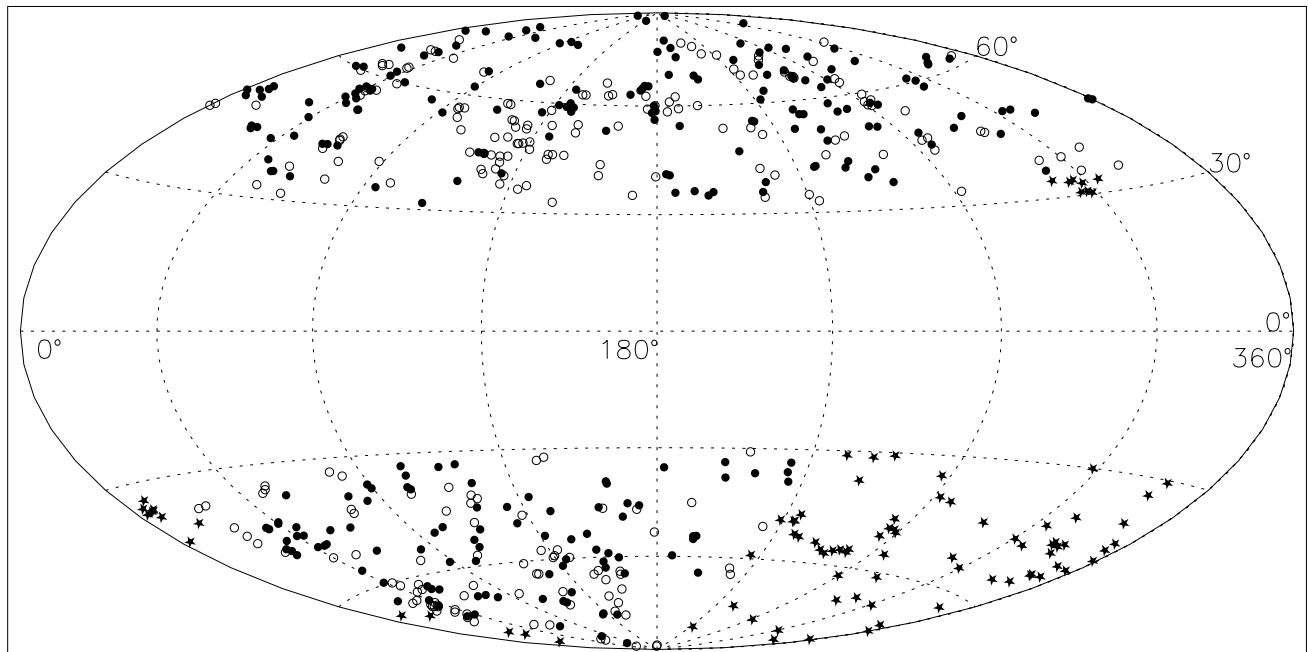


FIG. 2.— A Hammer-Aitoff projection sky-plot of all clusters used in the power spectrum analysis. Closed circles denote Abell (1958) clusters within $z = 0.10$, open circles denote Abell clusters with $0.10 < z \leq 0.14$, and stars indicate ACO (1989) clusters within $z = 0.10$. We have divided our sample into four quadrants in latitude/longitude and two bins in z , to show that the clusters in our sample have been observed evenly throughout the sky (see Table 1).

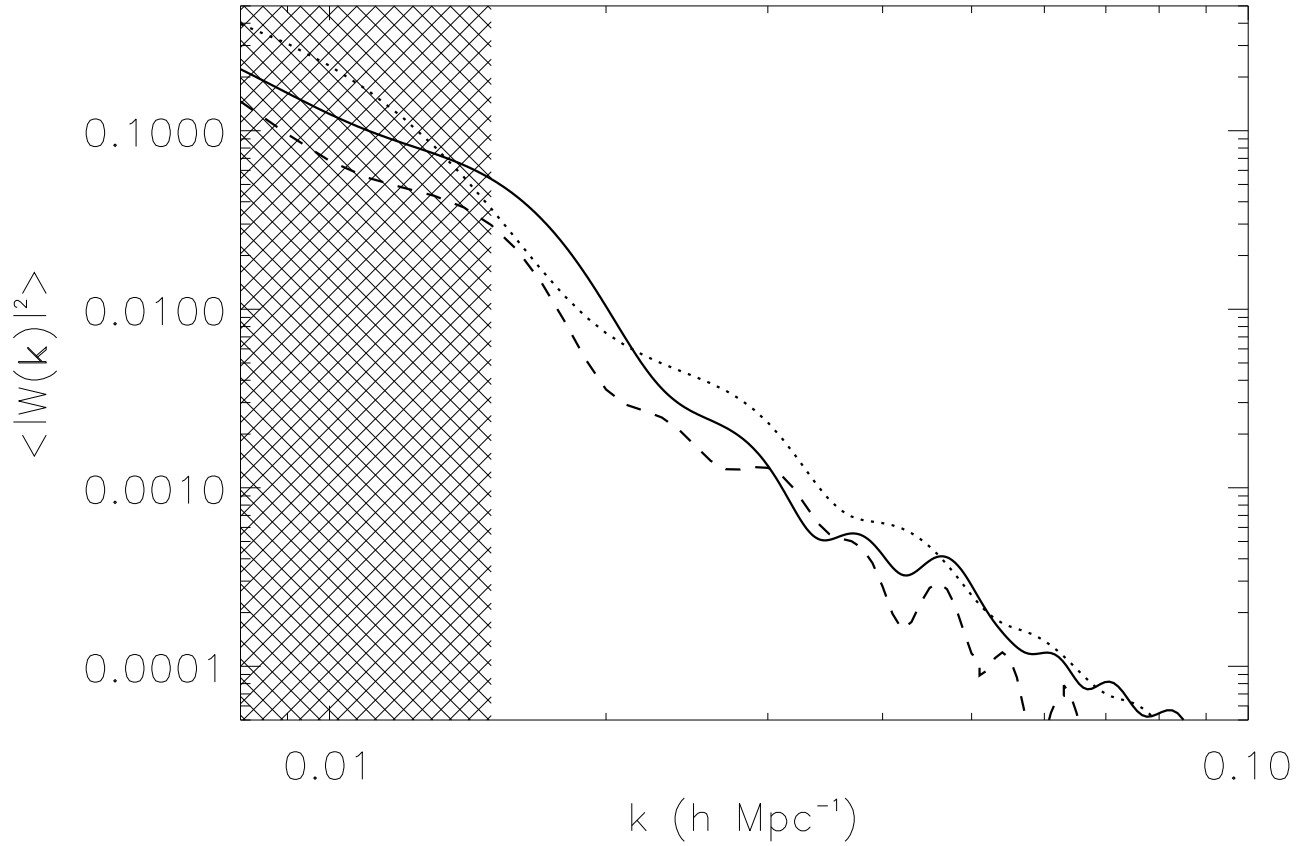


FIG. 3.— This is the Fourier window function, $\langle |\hat{W}(\mathbf{k})|^2 \rangle$ used to calculate $P_a(k)$. We use 300000 points and 1000 random directions for each $|k|$ to estimate the Fourier transform of the window function. k is in units of $h\text{Mpc}^{-1}$. The dashed-line is for a random distribution of points. The solid-line is after we apply the same redshift and extinction distribution as our real data. The dotted-line is for a highly asymmetric survey (i.e. one hemisphere to $z = 0.14$). The hatched region indicates where our window function prevents an accurate determination of $P(k)$.

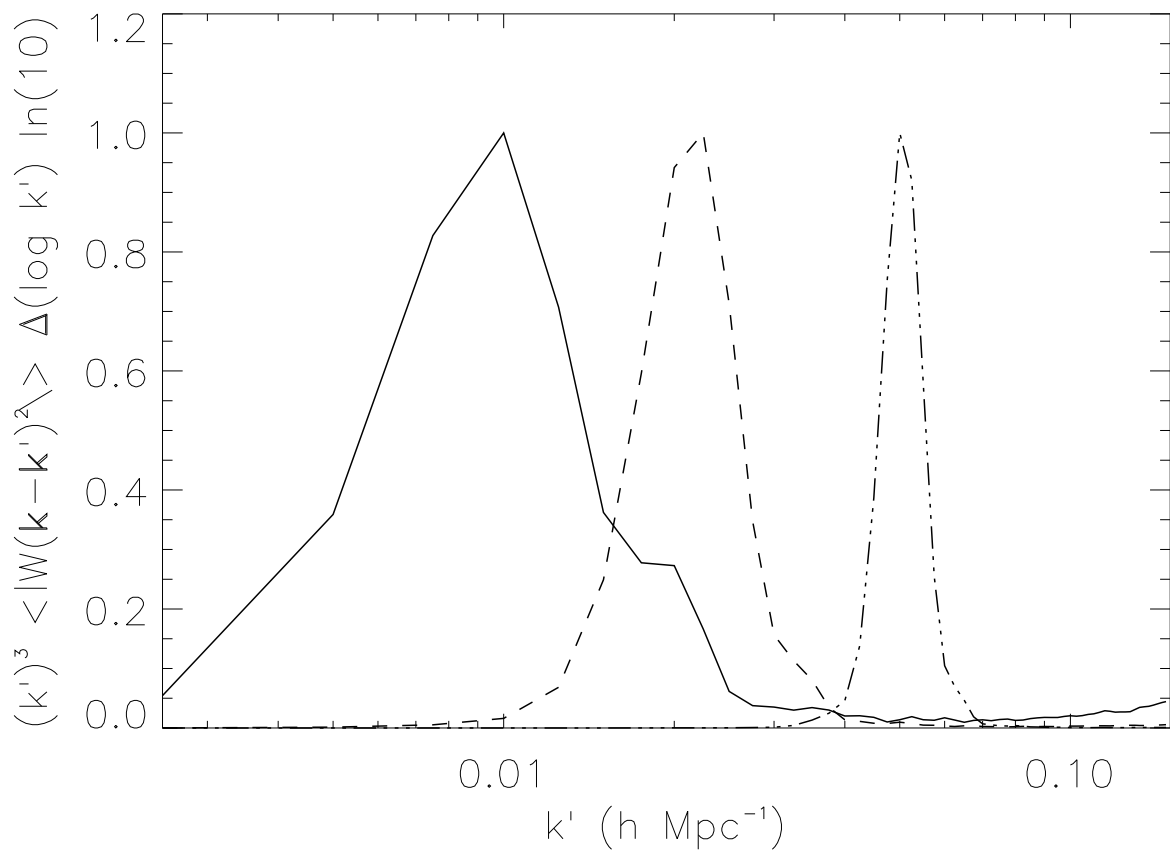


FIG. 4.— The integrand of Equation (2) for constant $P(k)$ with arbitrary normalization. We show three values of $k = 0.01, 0.02, 0.05 h\text{Mpc}^{-1}$. We see that for $k = 0.01 h\text{Mpc}^{-1}$ there is “leakage” from large k . At $k = 0.02 h\text{Mpc}^{-1}$ this leakage is no longer evident, and so we choose $k_{min} = 0.015 h\text{Mpc}^{-1}$ as the largest-scales we can accurately probe.

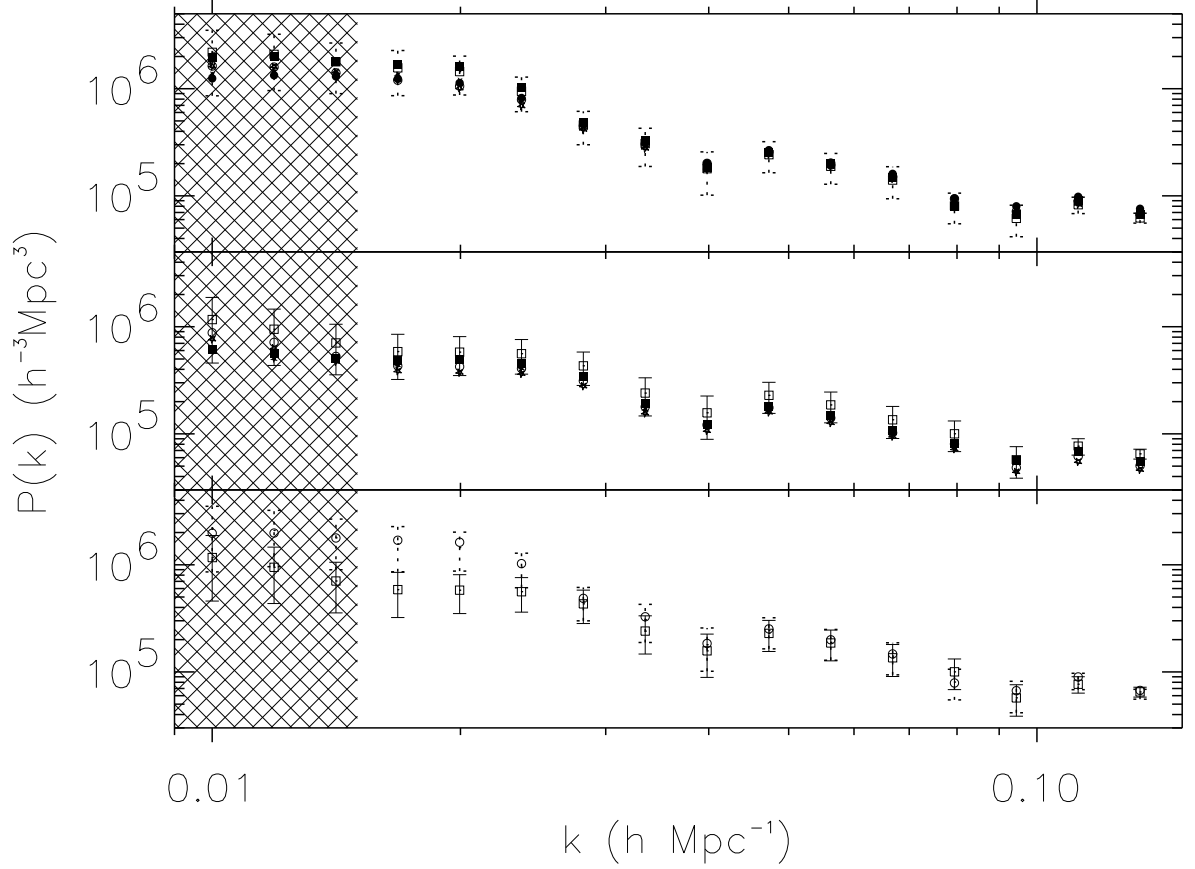


FIG. 5.— In the **top** panel we show $P_a(k)$ calculated using the three different number density functions used in Figure 1. Circles are for the step-function, stars are for the power-law fit, and squares are for the number function fit. The open circles include all $R \geq 1$ ACO clusters while the filled symbols are for ACO clusters with $N_{gal} \geq 56$. We use a window function that models the real data (e.g. in density and extinction). The errors are estimates based on scaling the errors from $P_b(k)$. In the **middle** panel we show $P_b(k)$ using the same symbols as the top panel. We use random catalogs with the same extinction and density distribution as the real data. The error bars are determined using the FKP method as mentioned in the text. In the **bottom** panel, we plot $P_a(k)$ (circles) and $P_b(k)$ (squares). The hatched region indicates where our window function prevents an accurate determination of $P(k)$.

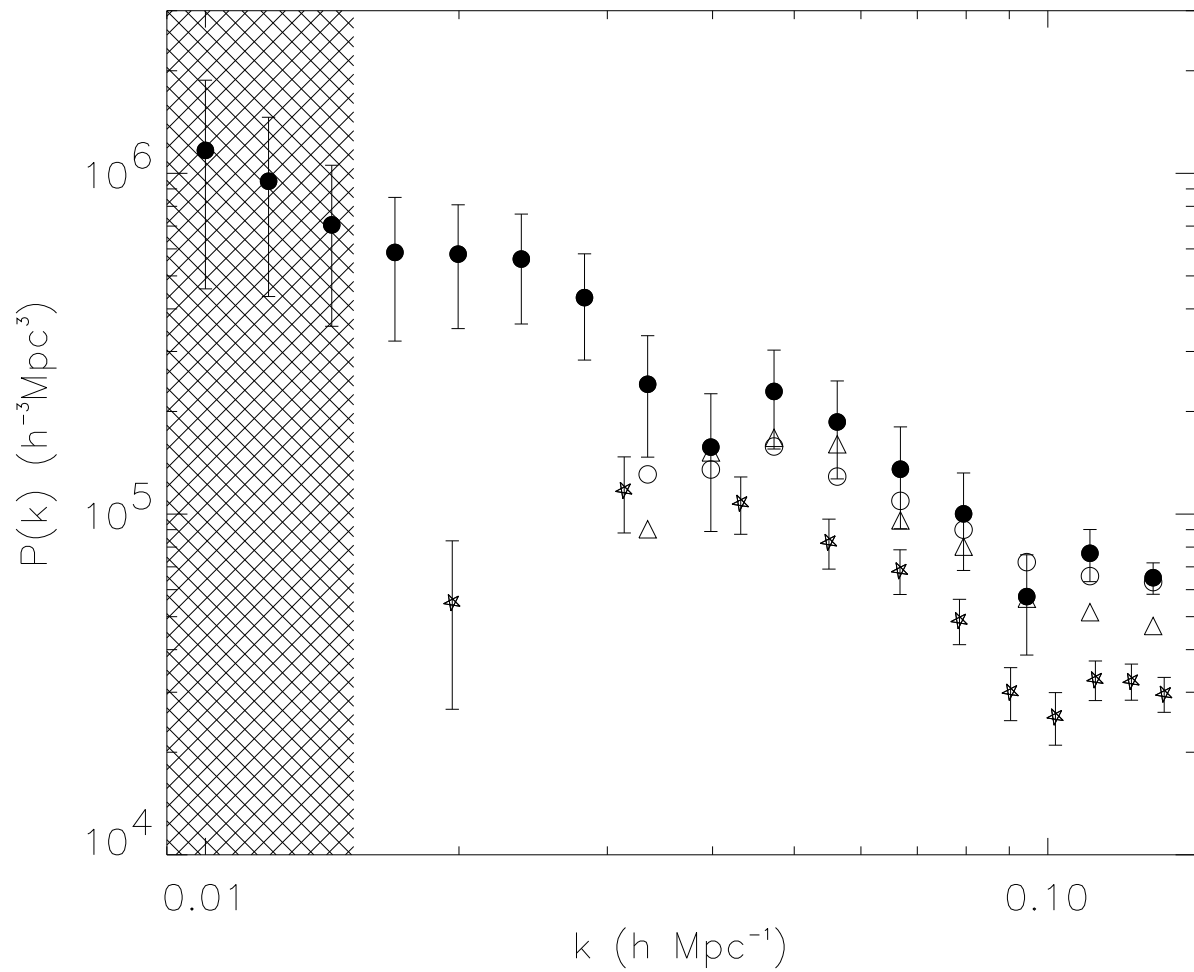


FIG. 6.— We compare $P_b(k)$ for Abell/ACO clusters calculated in this work (solid circles) to the smaller Abell/ACO sample used by Retzlaff *et al.* (1998) (triangles) and the APM cluster sample power spectrum calculated by Tadros *et al.* (1998) (stars). The open circles are $R \geq 1$ Abell/ACO clusters within $z = 0.10$ (north and south).

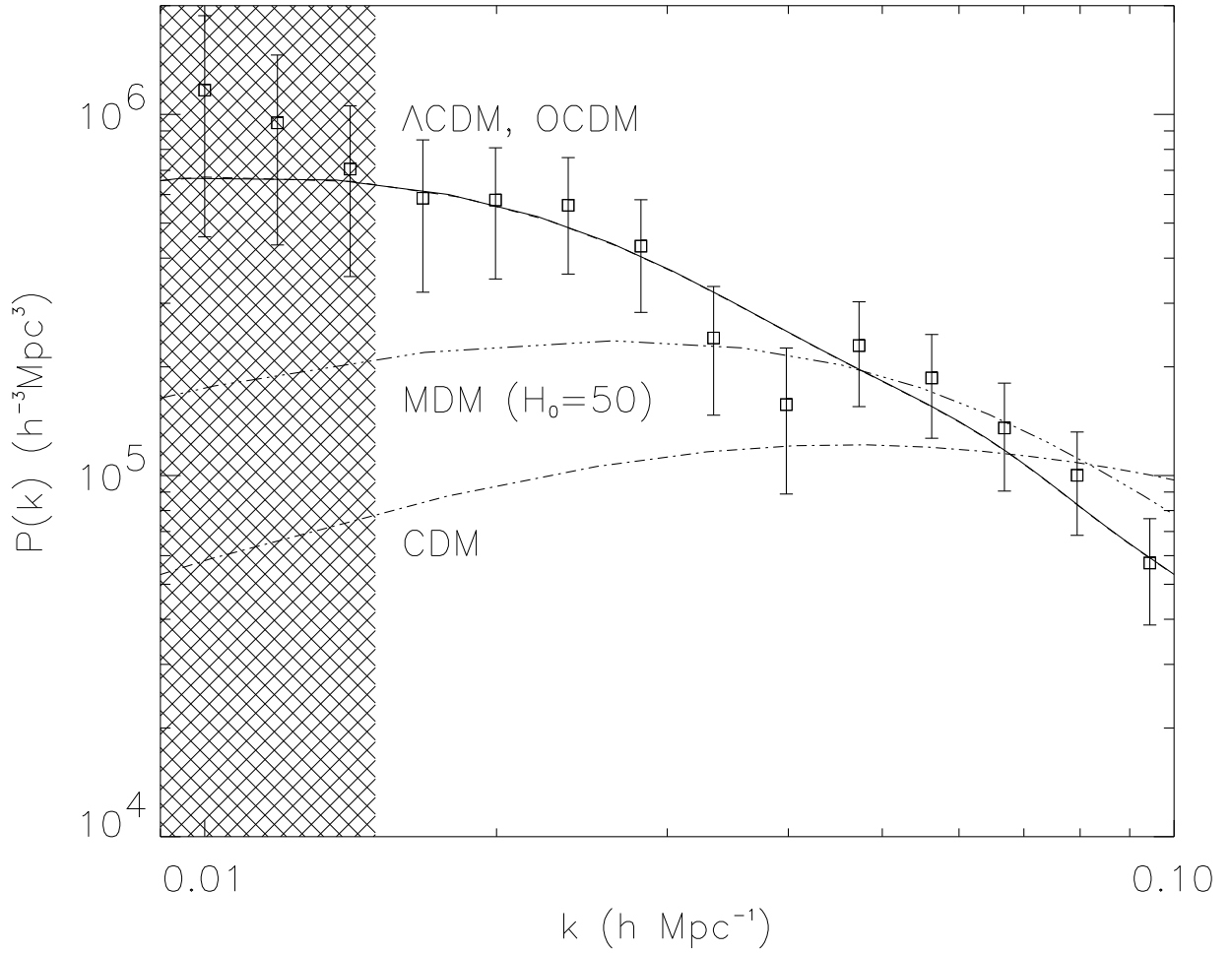


FIG. 7.— We compare $P_b(k)$ to model linear power spectra for a flat CDM ($\Omega_b = 0.02, \Omega_{CDM} = 0.98$ with $H_0 = 100 \text{km s}^{-1} \text{Mpc}^{-1}$ **dashed-dot**), mixed dark matter ($\Omega_b = 0.05, \Omega_{CDM} = 0.65$ and $\Omega_\nu = 0.3$ with $H_0 = 50 \text{km s}^{-1} \text{Mpc}^{-1}$ **dashed-dot-dot**), open ($\Omega_b = 0.02, \Omega_{CDM} = 0.18$ with $H_0 = 100 \text{km s}^{-1} \text{Mpc}^{-1}$ **dashed**), and lambda ($\Omega_b = 0.02, \Omega_{CDM} = 0.18, \Omega_{vacuum} = 0.80$ **solid**) CDM models.